Destabilization of the Tumor-Inducing Plasmid from an Octopine-Type *Agrobacterium tumefaciens* Lineage Drives a Large Deletion in the Co-Resident At Megaplasmid

Ian S. Barton[†], Thomas G. Platt[‡], Douglas B. Rusch[§] and Clay Fuqua[†*]

[†]Department of Biology
Indiana University
Bloomington, Indiana, USA

[‡]Division of Biology
Kansas State University
Manhattan, KS 66506

[§]Center for Genomics and Bioinformatics
Indiana University
Bloomington, IN 47405

Running Title: Megaplasmid deletion in *Agrobacterium*

Keywords: Ti plasmid, accessory genome, plasmid curing, deletion, IS element, conjugal transfer

*Address for correspondence: Clay Fuqua, Dept. Biol., 1001 E. 3rd St., Jordan Hall 142, Indiana Univ., Bloomington, IN 47405-1847. Tel: 812-856-6005, FAX: 812-855-6705, E-mail: cfuqua@indiana.edu

ABSTRACT

Bacteria with multi-replicon genome organizations, including members of the family *Rhizobiaceae*, often carry a variety of niche-associated functions on large plasmids. While evidence exists for cross-replicon interactions and co-evolution between replicons in many of these systems, remarkable strain-to-strain variation is observed within secondary replicons, suggesting environment-dependent fitness benefits of the accessory genome. Here, we show that curing of the tumor-inducing virulence plasmid (pTi) of an octopine-type *Agrobacterium tumefaciens* lineage drives a large deletion in the co-resident At megaplasmid (pAt). The deletion event is mediated by a repetitive IS-element, IS66, and results in a variety of environment-dependent fitness consequences, including loss of independent conjugal transfer of the plasmid. Interestingly, a similar deletion event is also found in a related *A. tumefaciens* strain, suggesting the mechanism is conserved in a subset of agrobacteria. Overall, the findings presented here uncover a novel genetic interaction between the two large plasmids of *A. tumefaciens* and provide evidence for cross-replicon integration and co-evolution of these plasmids.

INTRODUCTION

Bacteria exhibit a diversity of genomic architectures and contain replicons that range from small, transient plasmids, to chromids, to secondary and primary chromosomes (diCenzo and Finan 2017). Approximately 10% of bacteria possess multi-partite genomes and it is hypothesized that this arrangement may allow increased genome size, faster growth rate, coordinated gene regulation, and adaptation to novel niches

23 (Chain et al. 2006, diCenzo et al. 2017, diCenzo et al. 2014, Galardini et al. 2013, Slater
24 et al. 2009). A multi-partite genome organization is likely maintained through selective
25 pressures, but factors affecting replicon stability and their dynamic interactions are not
26 well understood and often vary significantly between and within species.

27 Secondary replicons such as megaplasmids and plasmids confer a variety of niche-
28 associated functions, such as antibiotic resistance, virulence, and symbiosis (diCenzo et
29 al. 2017, Funnell et al. 2004). While many of these replicons are dispensable in the
30 laboratory, they often have profound positive and negative effects on bacterial fitness in
31 a variety of environments and can affect growth rate and competition (diCenzo et al.
32 2017, diCenzo et al. 2014, Finan et al. 1986, Morton et al. 2013, Morton et al. 2014), as
33 well as numerous other phenotypes (Dougherty et al. 2014). Fitness consequences
34 resulting from gain or loss of accessory genes and replicons are not typically measured,
35 but likely depend on a combination of factors, including energetic demands of DNA
36 replication, transcription and expression of specific costly functions, such as ABC
37 transporters, as well as interactions between regulatory networks and pathways across
38 replicons (diCenzo et al. 2017, Mauchline et al. 2014, Morton et al. 2013, Romanchuk et
39 al. 2014).

40 Cross-replicon interactions and genetic regulation are both a consequence of and a
41 limitation to stabilization of secondary replicons and have been observed in diverse
42 bacterial species, including species of *Vibrio* (Heidelberg et al. 2000, Ramachandran et
43 al. 2017) and *Sinorhizobium* (Barnett et al. 2004, Bobik et al. 2006, diCenzo et al. 2018,
44 Galardini et al. 2015, Pini et al. 2015, Ronson et al. 1987). In most cases, chromosomal
45 factors influence the regulation of secondary replicon factors, with limited regulation in

46 the opposite direction (Agnoli et al. 2012, Barnett et al. 2004, Bobik et al. 2006, diCenzo
47 et al. 2018, Galardini et al. 2015, Pini et al. 2015, Ronson et al. 1987), likely due to
48 intolerance of integral pathway perturbation and the suppression of costly accessory
49 functions required to stabilize secondary replicons. However, metabolic redundancy has
50 been observed between rhizobial replicons (diCenzo et al. 2017, González et al. 2005),
51 suggesting that favorable interaction and pathway integration between primary and
52 secondary replicons occurs. However, because the majority of organisms possessing
53 multi-partite genomes exist and transition between multiple environmental reservoirs,
54 and are often host-associated, the extent to which cross-replicon interactions occur and
55 their consequences are often not determined.

56 Here, we characterize a cross-replicon genetic interaction in an octopine-type lineage of
57 the plant pathogen *Agrobacterium tumefaciens,* causative agent of crown gall disease
58 on plants (Escobar et al. 2003, Van Larebeke et al. 1974, Watson et al. 1975). We
59 observe that the process of curing the tumor-inducing (Ti) virulence plasmid drives a
60 large deletion in the co-resident At megaplasmid of the octopine-type *A. tumefaciens*
61 strain 15955. The deletion event is mediated by a repetitive IS-element and results in
62 variety of environment-dependent fitness consequences. Interestingly, the deletion
63 observed here is also present in the genome sequence of a related *A. tumefaciens*
64 strain, suggesting that the deletion mechanism described here is common to a subset of
65 strains in the *A. tumefaciens* genomospecies complex. Overall, the findings presented
66 here indicate a novel and complex genetic interdigitization of these two large plasmids
67 in *A. tumefaciens* and provides mechanistic precedent for the stabilization of and cross-
68 replicon interactions between rhizobial plasmids.

69 **MATERIALS AND METHODS**

70 **Reagents, media, strains, and growth conditions**

71 All strains and plasmids used in this study are described in Table S1. Specific
72 oligonucleotides are listed in Table S2, and all oligonucleotides used in the study are
73 available upon request. Chemicals, antibiotics, and culture media were obtained from
74 Fisher Scientific (Pittsburgh, PA), Sigma-Aldrich (St. Louis, MO), and GoldBio (St.
75 Louis, MO) unless otherwise noted. Plasmid design and verification as well as strain
76 creation was performed as described previously (Morton et al. 2012) with specific
77 details included in the text. Oligonucleotide primers were ordered from Integrated DNA
78 Technologies, Coralville, IA. Single primer extension DNA sequencing was performed
79 by ACGT, Inc., Wheeling, IL. Plasmids were introduced into *E. coli* via transformation
80 with standard chemically competent cell preparations and into *A. tumefaciens* via
81 electroporation or conjugation (Morton et al. 2012).

82 *E. coli* was cultured in standard LB broth with or without 1.5% (w v^{-1}) agar. Unless noted
83 otherwise, *A. tumefaciens* strains were grown on AT minimal medium containing 0.5%
84 (w v^{-1}) glucose and 15 mM ammonium sulfate without added $FeS0_4$ (ATGN) (Morton et
85 al. 2012), or AT with 5% (w v^{-1}) sucrose as the sole carbon source (ATSN). When
86 required, appropriate antibiotics were added to the medium as follows: for *E. coli*, 100
87 µg ml^{-1} ampicillin (Ap), 50 µg ml^{-1} gentamicin (Gm), and 50 µg ml^{-1} kanamycin (Km); and
88 for *A. tumefaciens*, 300 µg ml^{-1} Gm, 300 µg ml^{-1} Km, and 300 µg ml^{-1} spectinomycin
89 (Sp). For competition experiments, *A. tumefaciens* 15955 strains were grown in replete
90 carbon (standard ATGN), limiting carbon (ATGN with 0.018% (w v^{-1}) glucose) or

91 virulence-inducing media (Modified ATGN, replacing AT buffer with 50 μM phosphate
92 buffer (NaH_2PO_4, Na_2HPO_4, pH 5.7) with 0.02M 2-N-[morpholino]ethanesulfonate
93 (MES), and supplementing with 200 μM acetosyringone (Morton et al. 2012). Octopine
94 utilization was evaluated by growing *A. tumefaciens* 15955 in AT media modified to
95 contain octopine (3.2 mM) as the sole carbon and nitrogen source (ATO).

96 Precise deletion of IS66 was achieved using a previously described method (Morton et
97 al. 2012). 500-750 bp of sequence upstream (P1 and P2) and downstream (P3 and P4)
98 of the gene to be deleted were amplified using Phusion polymerase (New England
99 Biolabs, Ipswich, MA). Primers P2 and P3 were designed with 5' sequences with
100 reverse complementarity to each other's 3' proximal sequence. The complementary
101 sequence on these two primers facilitated splicing by overlapping extension (SOE) of
102 the two PCR products, as previously described (Morton et al. 2012). Both flanking
103 sequences were amplified and gel purified. The two purified products were then used as
104 both templates and primers in a second PCR reaction, generating the final spliced
105 product, which was ligated into pGEM-T easy (Promega) and sequenced to ensure
106 proper splicing. The deletion construct was then excised using restriction enzymes and
107 ligated into the suicide vector pNPTS138 cleaved with compatible restriction enzymes.
108 The pNPTS138 plasmid confers Km resistance (Km^R) and sucrose sensitivity (Suc^S).
109 Derivatives of pNPTS138 were introduced into *A. tumefaciens* 15955 by mating with *E.*
110 *coli* S17-1/λpir carrying the appropriate construct. The ColE1 origin of pNPTS138 does
111 not replicate in *A. tumefaciens*, necessitating single-crossover integration into the
112 chromosome to obtain Km^R transformants. Plasmid integration was confirmed by
113 patching onto ATGN-Km and ATSN to identify Suc^S derivatives. Excision of the

114 integrated plasmid was then mediated by growing overnight cultures of Suc^S Km^R
115 derivatives and plating dilutions onto ATSN. Plasmid excision was confirmed by
116 patching Suc^R clones onto ATSN and ATGN-Km to identify Km^S derivatives. Correct
117 deletion of the target gene was confirmed via diagnostic PCR using primers (P5/P6)
118 flanking the deletion site.

119 Marked derivatives of *A. tumefaciens* 15955 were created using an approach similar to
120 the creation of in-frame deletions (above) with minor alterations. P2 and P3 were
121 designed to have complementarity in the form of a multiple cloning site, consisting of
122 five restriction sites. After splicing of the PCR-amplified product into pNPTS138, the
123 restriction sites were used to fuse in different screenable and selectable markers.
124 Plasmid excision in Km^S derivatives of Suc^R clones were confirmed similarly, and
125 retention of the screenable or selectable markers was verified by sequencing of PCR
126 products.

127

128 **Whole genome sequencing and bioinformatic analysis**

129 Whole genome sequencing and assembly was performed at the Center for Genomics
130 and Bioinformatics, Indiana University, Bloomington, IN. WT *A. tumefaciens* 15955 was
131 sequenced and assembled *de novo* using a combination of 454 and Illumina NextSeq
132 platforms. Sequencing of *A. tumefaciens* 15955 derivatives was performed using
133 Illumina NextSeq 300 with 150 bp paired-end read libraries. Raw reads were trimmed
134 using Trimmomatic ver. 0.33 (Bolger et al. 2014) and mapped to the assembled WT *A.*
135 *tumefaciens* 15955 genome (above) using bowtie2 ver. 2.2.6 (Langmead et al. 2012).

136 Mapping efficiency was >99% and concordantly mapped reads had an average insert
137 size of ~500 bp with a normal distribution. Average coverage across the genome was at
138 least 20X. Variation between WT *A. tumefaciens* 15955 and derivatives were
139 determined using breseq ver. 0.24rc6 (Deatherage et al. 2014). Genome alignments
140 and comparisons were performed with mummer and mummerplot packages of
141 MUMmer 3.23 (Kurtz et al. 2004) and Artemis Comparison Tool (ACT) (Carver et al.
142 2005) visualizations of TBLASTX (https://blast.ncbi.nlm.nih.gov/Blast.cgi) data.
143 Toxin/anti-toxin searches were performed using TAfinder
144 (http://202.120.12.133/TAfinder/index.php) (Xie et al. 2018). Over the course of this
145 project a group from the Academia Sinica in Taiwan deposited a complete genome
146 sequence for the wild type *A. tumefaciens* 15955 into GenBank (Accession numbers;
147 Bioproject PRJNA494475; Circular chrom. NZ_CP032917.1; Linear chrom.
148 NZ_CP032918.1; pAt15955 NZ_CP032919.1; pTi15955 NZ_CP032920.1). This
149 sequence is in near-perfect agreement with our de novo wild type sequence, and we
150 refer to the coordinates of this deposited sequence where relevant.

151 **Southern blotting**

152 A ~500 bp DIG-labeled DNA probe (Sigma-Aldrich) specific to IS66 was generated with
153 PCR (1:6 ratio dig-UTP:dTTP) using primers IBP102/IBP103 and used to probe 2.5 µg
154 restriction digested gDNA (*Sph*I, *Eco*RI, *Bam*HI) that had been electrophoresed on a
155 0.75% agarose gel (2h, 50V) and transferred to a charged nylon membrane via capillary
156 blotting under alkaline conditions, as described previously (Fuqua et al. 1993).
157 Restriction digests were performed at 37°C for 2 hours. Hybridizations and detection of

158 the DIG-labeled DNA probe were performed according to manufacturer's suggestions
159 (Sigma-Aldrich). Blots were visualized using a Bio-Rad Chemidoc.

160 **pTi15955 curing and detection of pAt15955 segment loss**

161 Curing of pTi15955 was performed as described by our lab previously (Morton et al.
162 2012) with slight modifications. The curing plasmid is similar to the pBBR1-type curing
163 plasmids recently described (Yamamoto et al. 2018), containing two origins capable of
164 replication in *Agrobacterium*, a Km^R cassette, and the counterselectable *sacB* marker
165 for removal of the curing plasmid. Briefly, pSRKKm was digested with *Bam*HI (NEB)
166 according with NEB guidelines, followed by purification using the E.Z.N.A. Cycle Pure
167 Kit from Omega Bio-tek. The digested and purified pSRKKm backbone was then used
168 in a three-part NEBuilder isothermal assembly reaction (New England Biolabs) with
169 *repABC* (pTi15955) and *sacB* PCR products that were amplified from *A. tumefaciens*
170 15955 gDNA or purified pNPTS138, respectively, using primer pairs IBP200/IBP201
171 and IBP202/203 to create pIB301. NEBuilder reactions were performed as specified by
172 the supplier using a 1:2 vector to insert ratio. pIB301 was confirmed using a
173 combination of PCR and sequencing.

174 pIB301 was introduced into *A. tumefaciens* 15955 backgrounds via conjugation from *E.*
175 *coli* S17-1/λpir donor and *A. tumefaciens* 15955 transconjugants were identified through
176 selective plating. Screening for pTi15955 curing and loss of the pAt15955 segment was
177 performed using loss of *gusA* or *lacZ* activity on 5-bromo-4-chloro-3-indolyl-β-
178 glucuronic acid (X-Gluc) or 5-bromo-4-chloro-3-indolyl-β-D-galactopyranoside (X-Gal)
179 as well as gentamicin or spectinomycin sensitivity, respectively, and/or a combination of

180 Eckhardt gel electrophoresis (Eckhardt 1978) and PCR. Eckhardt gel electrophoresis
181 was performed according to a modified protocol (Personal communication, J. Griffitts,
182 Brigham Young University, Provo, UT). Additionally, the presence of pTi15955 was also
183 evaluated using octopine auxotrophy screening.

184 **Ti plasmid reintroduction and conjugation assays**

185 pTi15955::*gusA/*Gm^R was reintroduced into Sp^R *A. tumefaciens* 15955 backgrounds
186 (IB128/IB129) through conjugation with IB123 (At+Ti+::*gusA*/Gm^R) as a donor in ATGN
187 media supplemented with octopine [3.25 mM]. Briefly, donor and recipients were grown
188 in ATGN supplemented with appropriate antibiotics to OD_{600} 0.6 and 100 µL of donor
189 and recipient were combined and spotted onto sterile 0.2 µm cellulose acetate filter
190 discs placed on ATGN media supplemented with octopine (ATGNO [3.25 mM]). After
191 incubation (18 h, 28°C), the spots were resuspended in ATGN and plated onto ATGN
192 supplemented with antibiotics to select for transconjugants. Transconjugants were
193 confirmed using Eckhardt gel electrophoresis and PCR.

194 Conjugation assays were performed as described previously (Heckel et al. 2014) with
195 alterations. Briefly, donors and recipient were grown and normalized to OD_{600} 0.6,
196 mixed 1:1, and 100 µL was spotted onto 0.2 µm cellulose acetate filter discs placed on
197 ATGN supplemented with and without octopine [3.25 mM]. Following incubation (18h,
198 28°C), matings were suspended in liquid ATGN, serially diluted, and spotted onto media
199 supplemented with appropriate antibiotics. Conjugation efficiency was determined as
200 the ratio of transconjugants per output donor.

201

202 **Truncation of pAt15955 segment using Cre-lox**

203 The *loxP* site (5'
204 GCGGTCGACATAACTTCGTATA*ATGTATGC*TATACGAAGTTATCATATGGCG 3', 18
205 bp inverted sequences are underlined, and the 8bp spacer is italicized) was introduced
206 into four locations within pAt15955::*lacZ*/Sp^R of IB118 in a pair-wise fashion to truncate
207 either half of, or the entire pAt15955 segment upon transient expression of the Cre
208 recombinase. To allow Cre-mediated deletion the left half of the At plasmid segment
209 (denoted L), *loxP* sites were introduced in a tandem, direct orientation into positions L
210 and CL that are interior to the flanking IS66 element and *lacZ*Sp^R marker in IB118,
211 respectively, to create IB118 *lox*L (Figure S5 and Table S1). Deletion of right half
212 (denoted R) of the segment was done similarly, except *loxP* sites were integrated at
213 positions CR and R to create IB118 *lox*R. *loxP* sites were integrated at positions L and
214 R to create IB118 *lox*L+R and allow deletion of the entire segment. Confirmation of
215 genomic integration of each *loxP* site was done using PCR with primers specific for
216 each integration site. Transient expression of the Cre recombinase was accomplished
217 through introduction of the pCRE1-Ap suicide vector (Bailey et al. 2002) into the
218 appropriate *A. tumefaciens* 15955 recipient (IB118 *lox*L, IB118 *lox*R, or IB118 *lox*L+R)
219 via mating with *E.coli* S17-1/λpir pCRE1-Ap as described [1] with minor alterations. After
220 mating of donor and recipients on LB agar, resuspensions were plated onto LB with or
221 without Sp supplementation for deletion of the left and right half or entire segment,
222 respectively. Confirmation of Cre-mediated deletions were confirmed using Eckhardt gel
223 electrophoresis and PCR with primers specific for each new junction site created
224 through Cre-mediated deletion.

225 **Competition experiments**

226 Competition experiments were performed as described previously with minor alterations
227 (Morton et al. 2013). Competitor strains were grown in ATGN with or without antibiotic to
228 an OD600nm of 0.6-0.8, washed 3 times in ddH_20, and mixed 1:1 at an OD600nm of
229 0.01 in 2 mL of media. When competitions reached an OD600 nm of 0.6-0.8, 0.4-0.6, or
230 0.2-0.4 for replete carbon, limiting carbon, and virulence-inducing media, respectively,
231 the competitions were serially diluted and spotted onto ATGN with and without antibiotic
232 to enumerate each competitor, as well as sub-cultured (1:100) into the same media.
233 Competitions were carried out for a total of nine passages and each was performed 3
234 times with reciprocally-marked strains for a total of 6 replicates. Relative fitness was
235 estimated as the number of doublings by each competitor over each passage during the
236 course of the experiment, as described previously (Lenski 1988, Morton et al. 2013).
237 Passaging intervals, such as P0-P9, thusly denote cumulative doublings over every
238 passage.

239 **Data and reagent availability.** The *A. tumefaciens* 15955 genome sequence is
240 available through GenBank Accession No. PRJNA494475, and all coordinates for this
241 genome sequence cited in the manuscript correspond to this sequence. All reagents,
242 including strains, plasmids, and oligonucleotides are available upon request
243 Supplementary information, including figures, tables and reference for this study have
244 been deposited as a single file in GSA figshare (filename:
245 pAt15955_Deletion_Supplementary_Info_040919).

246

247 **RESULTS**

248 **Large deletion in pAt15955 upon pTi15955 curing.**

249 Several on-going studies rely on curing of the Ti plasmid from *A. tumefaciens*, using a
250 plasmid incompatibility, eviction process (Platt et al. 2012, Uraji et al. 2002, Yamamoto
251 et al. 2018). As a matter of practice, the plasmid profiles of putatively cured derivatives
252 are analyzed by Eckhardt gel electrophoresis to visualize their large plasmid content
253 (see Materials and Methods). Eckhardt gel analysis of *A. tumefaciens* 15955 revealed
254 two discrete bands, reflecting the presence of both an At plasmid (pAt15955, large
255 band) and Ti plasmid (pTi15955, smaller band) (Figure 1). Several derivatives of *A.*
256 *tumefaciens* 15955 were cured of their Ti plasmid using the incompatibility-eviction
257 approach. Strikingly, it was observed that these cured derivatives of *A. tumefaciens*
258 15955 lost the Ti plasmid, but also lost the pAt band, replaced by a plasmid species that
259 migrated faster than pAt but more slowly than pTi (Figure 1). This change in plasmid
260 profile was observed for virtually all of the Ti plasmid-cured derivatives from multiple
261 experiments, and suggested that the pAt plasmid had incurred a large deletion
262 coincident with loss of the Ti plasmid. Interestingly, Eckhardt gel analysis of *A.*
263 *tumefaciens* SA122, a 15955 derivative cured by a completely different approach using
264 chemical and temperature stress in a different laboratory years earlier revealed the
265 same pattern as the derivatives we had generated (Figure 1, and see Materials and
266 Methods) (Uraji 2002, Yamamoto et al. 2018).

267 To confirm loss of pTi15955, as well as diagnose other genomic changes in these
268 strains underlying the changes observed using Eckhardt gel electrophoresis, whole

genome sequencing was conducted on WT *A. tumefaciens* 15955 and pTi15955-cured derivatives. WT *A. tumefaciens* 15955 assembled into 13 scaffolds, the first four corresponding to the circular chromosome (scaffold00001, 2.836 Mbp), linear chromosome (scaffold 00002, 2.082 Mbp), pAt (scaffold00003, 0.816 Mbp), and pTi (scaffold00004, 0.192 Mbp). Nine other smaller scaffolds did not assemble with the four primary scaffolds and ranged in size from 16.045 Kbp (scaffold00005) to 2.419 Kbp (scaffold00013). The sequencing readily confirmed loss of pTi15955 in cured derivatives but also identified a large (270,949 bp) deletion in the pAt15955 (Figure 2) that was consistent between multiple pTi15955-cured isolates (Figure 2 and data not shown). From this, we concluded the single band present in pTi15955-cured isolates upon Eckhardt gel electrophoresis is the truncated pAt15955 (denoted as pAt15955Δ270) (Figure 1). The *A. tumefaciens* 15955 genome sequence recently deposited in GenBank database (Bioproject PRJNA494475) does not have this deletion, and matches our de novo generated wild type sequence.

Evaluation of curing and deletion frequencies suggests these processes are linked but independent.

We have observed two separate, large scale genomic events, Ti plasmid curing and the large deletion incurred in pAt15955, occurring coincidentally. To characterize the connection between these events, the correlation between pTi15955 curing and pAt15955 segment loss was determined under pTi15955 curing conditions. Incompatibility-based curing strategies were used to correlate both events due to the high frequency of curing using this method (Uraji 2002, Yamamoto et al. 2018). Using this strategy, a broad host range plasmid (pBBR origin) containing a copy of the

292 pTi15955 replication origin (*repABC*), a selectable kanamycin resistance marker (Km^R),
293 and a counterselectable marker (*sacB*) is introduced into *A. tumefaciens* 15955 strains
294 via conjugal transfer from an *E. coli* donor and the resulting transconjuants that exhibit
295 appropriate antibiotic resistance were screened for the loss of the Ti plasmid. Ti
296 plasmids generally have a low copy number under standard laboratory conditions
297 (Pappas 2008, Platt et al. 2014, Suzuki et al. 2001). Consequently, the presence of an
298 additional copy of the Ti plasmid replication origin on a higher copy number plasmid can
299 prevent proper maintenance and segregation of the Ti plasmid and lead to itsloss. The
300 pTi15955 curing vector used here is similar to those described previously (Platt et al.
301 2012, Uraji 2002, Yamamoto et al. 2018) and detailed in the Materials and Methods.

302 To increase the efficiency by which both curing of pTi15955 and loss of the pAt15955
303 segment could be diagnosed, screenable and selectable marker cassettes were
304 introduced into the *A. tumefaciens* 15955 genome within the pAt15955 segment (pos.
305 364,474) and on pTi15955 (pos. 17,447) using recombinational mutagenesis strategies
306 described previously (Morton et al. 2012). A *lacZ*/Sp^R cassette and a *gusA*/Gm^R
307 cassette were introduced between convergently oriented genes within the pAt15955
308 deletion segment and on pTi15955, respectively, to create IB118. Upon introduction of
309 the curing plasmid, frequencies for loss of the pAt15955 segment and pTi15955 curing
310 were determined through a combination of blue/white screening on X-Gal (β-
311 galactosidase, LacZ indicator) or X-Gluc (β-glucuronidase, GusA indicator), followed by
312 confirmation with Sp^S or Gm^S screening, respectively, and confirmed PCR and Eckhardt
313 gel analysis. Loss of LacZ or GusA activity and Sp or Gm sensitivity in these reporter

314 strains faithfully reported on pAt15955 segment loss or pTi15955 curing, respectively
315 (data not shown).

316 Using the *A. tumefaciens* 15955-IB118 derivative with the *lacZ*/Sp^R and a *gusA*/Gm^R
317 cassettes, it was determined that ~20% of curing plasmid transconjugants have lost
318 pTi15955 under assay conditions (Table 1). Consistent with previous analyses of
319 pTi15955-cured isolates (Figure 1), ~100% of pTi15955-cured isolates also incur loss of
320 the pAt15955Δ270 segment (Table 1). However, ~71% of curing plasmid
321 transconjugants incur loss of the segment, indicating that it is deleted at a higher
322 frequency than loss of the pTi15955 plasmid under these conditions (Table 1). Taken
323 together, the correlation suggests that curing conditions stimulate pTi15955 curing and
324 pAt15955 segment loss, that the events are separable, and that loss of the pAt15955
325 may precede, and/or possibly even limit, pTi15955 curing.

326 The frequencies observed above are consistent with a model in which a canonical
327 toxin/anti-toxin (TA) module is separated between the pTi and pAt replicons, where an
328 unlinked toxin on the pAt15955 segment and an anti-toxin on pTi15955 accounts for the
329 observation that pAt15955 segment loss precedes pTi15955 curing. Although sequence
330 searches using TAfinder (http://202.120.12.133/TAfinder/index.php) were able to
331 identify putative TA systems on both pAt15955 and pTi15955 (Table S4), no separable,
332 unlinked TA systems were identified using these programs. In general, a variety of
333 genetic interactions between the pAt15955 segment and pTi15955 could function as TA
334 systems, including cross-regulation of costly genes. For example, genomic stability may
335 be undermined following pAt15955Δ270 deletion if this results in loss of regulatory
336 repression of a costly factor encoded by pTi15955. These types of genetic interactions

337 would be difficult to identify via bioinformatic analysis and may depend on undetermined
338 environmental conditions. Interestingly, plasmid stabilization genes identified on
339 pAt15955 were enriched outside of the deletion interval (Table S4), which may partially
340 explain the propensity to lose this particular segment.

341 We also explored whether more general stress conditions could induce the observed
342 pAt15955 deletion. Multiple individual isolates of *A. tumefaciens* 15955 isolates grown
343 under standard conditions, antibiotic exposure, heat shock (37°C), and virulence-
344 inducing conditions (acidic pH and plant phenolics) were examined for the deletion.
345 None of the isolates tested (~3.0×10^8) had incurred the deletion suggesting that it is
346 specifically induced by the curing process, although independent of the exact curing
347 mechanism. This observation suggested that the loss is specific to conditions which
348 directly compromise replication of pTi15955 and may represent a genetic and functional
349 link between both replicons (Table 1 and data not shown).

350 ***A. tumefaciens* Ach5, an octopine-type strain that lacks the deleted pAt segment.**

351 Strains belonging to the *A. tumefaciens* species complex have been classified based on
352 their genome sequences into several genomospecies (Mougel et al. 2002), and *A.*
353 *tumefaciens* 15955 falls into the G1 genomospecies (Henkel et al. 2014, Huang et al.
354 2015). *A. tumefaciens* Ach5 is another G1 genomospecies with an octopine-type Ti
355 plasmid. Analysis of the Ach5 genome sequence (GenBank Access. No. Bioproject
356 PRJNA278497) reveals that is missing the exact same large segment as we have
357 observed to delete in 15955 under Ti plasmid curing conditions, with nearly identical
358 sequence flanking this region (Figure S1) (Henkel et al. 2014, Huang et al. 2015). This

359 suggests that the genomic lability of this segment has been manifested during the
360 evolutionary history of Ach5, and that the propensity for the deletion event may be
361 conserved within this subgroup of *A. tumefaciens* isolates.

362 **The pAt15955 deletion event is mediated by flanking IS66 elements.**

363 Analysis of whole genome sequencing data identified three copies of an IS element,
364 IS66, within the *A. tumefaciens* 15955 genome, one on the linear chromosome (pos.
365 28,096-30652) and two on pAt15955 (IS66_At_L, pos. 508,310-510,865 and
366 IS66_At_R, pos. 237,361-239,916), flanking the deletion interval (Figure S2). IS66
367 represents a family of IS elements conserved within a wide variety of bacteria, but was
368 first identified on an octopine-type Ti plasmid within *A. tumefaciens* (Gourbeyre et al.
369 2010, Han et al. 2001, Machida et al. 1984). The element consists of three open reading
370 frames, *tnpABC*, the latter of which is thought to encode an active transposase and is
371 the most conserved across the IS66-family. The three ORFs are bordered by distinct
372 direct and indirect repeats (Figure S2).

373 Repetitive sequences, such as IS-elements, are notoriously difficult to correctly
374 assemble in next generation sequencing data. We aimed to confirm and enumerate the
375 IS66 elements within *A. tumefaciens* 15955 and its deletion derivative using a Southern
376 blot approach (in our de novo sequencing, prior to the deposit of the curated 15955
377 genome sequence, the number of IS66 copies was uncertain). A 515 bp DNA fragment
378 specific for *tnpC* was generated by PCR (primers IBP102 and IBP103) and used to
379 probe restriction enzyme-digested genomic DNA (*Sph*I, *Eco*RI, and *Bam*HI) from *A.*
380 *tumefaciens* 15955 and its derivatives. In WT *A. tumefaciens* 15955 gDNA, three

381 distinct bands were present in restriction digests, confirming that *A. tumefaciens* 15955
382 contains three copies of IS66 (Figure 3A). Fragment sizes of detected bands are
383 consistent with two IS66 elements flanking the pAt15955 segment (Figure 3D).
384 Strikingly, only two visible bands are detectable for gDNA from the IBE13A derivative,
385 deleted for the At15955Δ270 plasmid segment, indicating loss of one IS66 element
386 during the deletion event (Figure 3B). One of the two fragments matches a fragment in
387 the wild type, and the second for the *Sph*I and *Eco*RI digests does not match either of
388 the other two restriction fragments in the wild type. The *Bam*HI digest of the deletion
389 mutant generates a predicted new fragment very close in size to the previous two.
390 These observations are consistent with loss of one IS66 element and retention of a
391 single copy of IS66 on pAt15955 at the site of deletion, and correlates with predictions
392 from our own sequence analysis (Figure 3D) and examination of the GenBank 15955
393 accession.

394 While nearly all *A. tumefaciens* 15955 curing plasmid transconjugants that lose
395 pTi15955 also lose the pAt15955 segment, we have recovered several rare isolates that
396 have been cured of pTi15955 but do not carry the deletion, including derivative
397 IBJUN138. Southern analysis of IBJUN138 did not deviate from the pattern observed for
398 *A. tumefaciens* 15955 (Figure 3C), confirming our sequence assemblies suggesting that
399 IS66 does not reside on the Ti plasmid in this strain and rather is on the linear
400 chromosome, in contrast to previous reports for IS66 on octopine-type Ti plasmids in
401 other *A. tumefaciens* strains (Machida et al. 1984).

402

403 Retention of a single IS66 element following the deletion event suggests homologous
404 recombination as the primary mechanism for segment deletion. Recombination-
405 mediated deletion of the pAt15955 segment would require that both elements be in the
406 same orientation (Petes et al. 1988). An inverse PCR approach was used to confirm
407 that both IS66 elements flanking the pAt15955 segment in WT *A. tumefaciens* 15955
408 exist in a tandem orientation (Figure S4A). Based on predicted restriction fragment
409 sizes surrounding each IS66 element in WT *A. tumefaciens* 15955, inverse PCR
410 products support the direct orientation of both elements (Figure S4B and data not
411 shown), also in agreement with the sequence assemblies.

412 As repetitive IS-elements are common substrates for homologous recombination, it
413 seemed likely that the two IS66 elements on pAt15955 were responsible for the
414 observed deletion during pTi15955 curing. To examine the role for both IS66 elements
415 in mediating the pAt15955Δ270 deletion, the left copy of the IS66 element (IS66-At-L)
416 was deleted from pAt15955 within the reporter strain IB118. The resulting strain
417 (IB118ΔIS66) was subjected to pTi15955-curing conditions and evaluated for pAt15955
418 segment loss and pTi15955 curing. The pAt15955Δ270 deletion event in IB118ΔIS66
419 under pTi15955 curing conditions was undetectable (Table 1), consistent with the
420 requirement for the two elements to drive homologous recombination. Interestingly, *A.*
421 *tumefaciens* Ach5 also has a single copy of IS66 at the deletion site in pAtAch5,
422 suggesting that IS66 may have mediated a similar large deletion in this strain (Figure
423 S3). Insertion of many transposable elements creates a short duplication at the site of
424 insertion, and this is reported to be 8 bp for IS66 (Machida et al. 1984). Unique 8 bp
425 duplications flank all three of the IS66 elements in the 15955 sequence (IS66_Lin,

426 AGAACACG; IS66_At_L, CCTTGATC; IS66_At_R, CGTTCCGG). In contrast, for the
427 pAt15955Δ270 deletion derivative the 8 bp sequences immediately flanking the left and
428 right ends in the single remaining At plasmid IS66 element match the outside flanking
429 sequence from the IS66_At_L and IS66_At_R, respectively (Fig. Sx). Similarly, the 8 bp
430 flanking each end of IS66 in pAtAch5 are different from each other (CCGGAACG and
431 CCTTGATC) and match those flanking the IS66 pAt15955Δ270. These observations
432 are again consistent with homologous recombination between IS66 elements driving the
433 deletion events in both the ancestor of pAtAch5 and in pAt15955.

434

435 **The pAt15955 segment has a modest but detectable stabilizing effect on pTi15955**

436 Our observations suggest a step-wise mechanism in which loss of the pAt15955
437 segment usually precedes pTi15955-curing (Table 1). However, we were able to obtain
438 a rare derivative in which the Ti plasmid was cured, but the pAt15955 plasmid did not
439 have the Δ270 deletion (IBJUN138). It seemed plausible that this derivative had
440 incurred mutations which abolished the mechanism by which loss of the Ti plasmid
441 stimulates the deletion event. However, whole genome sequence analysis of IBJUN138,
442 did not reveal mutations within the deleted segment and none that would readily explain
443 retention of this pAt segment (data not shown). We therefore used the IBJUN138 strain
444 that had retained the intact At plasmid but was cured for the Ti plasmid, to examine the
445 impact of the retained At plasmid genes on curing frequencies. The *gusA*/Gm^R-marked
446 pTi15955 plasmid was reintroduced by conjugation back into two pTi15955-cured
447 derivatives with a chromosomal Sp^R marker, one that had incurred loss of the pAt15955

448 segment (IB129) and another that had not (IB130, a derivative of IBJUN138) (Table S1
449 and Methods). These strains were then subjected to pTi15955-curing conditions and
450 evaluated for Ti plasmid loss. The reintroduction strain, IB130, appeared to have a
451 significant decrease in pTi15955 curing relative to other strains, and the IB129 strain
452 that had already incurred the pAt15955 deletion was modestly elevated in pTi curing
453 frequency (Table 1). These findings suggested that the presence of the pAt deletion
454 segment may stabilize the Ti plasmid.

455 We sought to determine whether the Ti plasmid stabilization was due to a specific
456 genetic locus within the deleted segment or tied to the carriage cost of this entire region.
457 To test this question, the derivative carrying the marker in the deleted segment (IB118)
458 was truncated for 138.8 kb on the left side (IB118 ∆L, pos. 504,337-365,531) or 106.7kb
459 on the right side (IB118 ∆R, pos. 354,236-247,489) portion of the deleted segment, or
460 the entire (IB118 ∆L+R) segment, using a Cre/*lox*-driven deletion approach (Figure S5,
461 Table S1, and Methods). Strains truncated with Cre/*lox* retain both flanking IS66 copies
462 and retain the *lacZ*Sp^R markers within the deletion interval, except for IB118∆L+R, in
463 which the *lacZ*Sp^R markers are deleted but flanking IS66 elements are still retained
464 (Figure S5). These engineered deletion derivatives were subjected to pTi15955-curing
465 conditions, and evaluated for pTi15955-curing frequencies. Truncation of part, or the
466 entire pAt15955 segment had modest, but measurable effects on pTi15955 stability
467 (Table 1). The two derivatives deleted for either the entire element or its right half
468 exhibited a modest increase in pTi15955 curing frequency, whereas the deletion of the
469 left half of this segment was very similar to the wild type frequency (Table 1). This
470 suggests that genetic elements within the right half of the pAt15955 segment may

471 influence pTi15955 stability (Table 1). Similar Ti plasmid curing frequencies were
472 observed for the isolated derivative deleted for the pAt15955 segment (IB129) with the
473 single IS66 element and the engineered derivative lacking the genes on the segment,
474 but retaining the tandem IS66 elements (IB118 ΔL+R), suggesting that the tandem IS66
475 elements alone do not influence pTi15955 stability (Table 1).

476 The modest alterations in pTi15955 stability in backgrounds with differing pAt15955
477 segment architectures suggests that the mechanism driving pAt15955 segment loss
478 may be influenced by the genetic content within the deleted segment (likely via genetic
479 elements in the right half of this segment), but this difference is unlikely to account for
480 the tight correlation between the pAt deletion event and Ti plasmid curing we have
481 observed.

482 **pAt15955Δ270 segment contains conjugation machinery and conjugation of**
483 **pAt15955 is octopine-inducible**

484 Analysis of whole genome sequence data from WT *A. tumefaciens* 15955 identified
485 conjugal transfer genes within pAt15955 that are homologous to functions on pTi15955
486 (Figure S6 and data not shown). Interestingly, unlike pTi15955 and other Ti plasmids,
487 pAt15955 *trb* and *traI* are not directly divergent from *repABC* and are rather encoded
488 within the AtΔ270 deletion segment (Figure S6). Thus, strains deleted for the pAt15955
489 segment are lacking *trb* and *traI* genes, which are essential for conjugation in Ti
490 plasmids with similar systems (Li et al. 1998, Li et al. 1999), and so they may be
491 incapable of conjugation. To test this, WT *A. tumefaciens* 15955 and derivatives that
492 lack the pAt15955 segment, pTi15955, or both, were marked with Km^R and used in

493 conjugation assays with the ERM52 recipient, a plasmidless (At^-Ti^-) *A. tumefaciens* C58
494 derivative marked with Sp^R (Figure 4, Methods). In standard growth conditions (ATGN),
495 low level At plasmid conjugation was observed for the marked wild type (IB125), and
496 this is abolished in the deleted derivative (At∆270 Ti^+) lacking the pAt15955 *trb* genes
497 (IB131). (Figure 4). Conjugation of the Ti plasmid in octopine-type *A. tumefaciens*
498 strains is strictly regulated by the presence of octopine and a complex quorum sensing
499 process (Fuqua et al. 1994, Gordon et al. 2014, Hwang et al. 1994, Piper et al. 1993).
500 Addition of octopine stimulates conjugal transfer frequency by two orders of magnitude
501 in the At^+Ti^+ donor (IB125). Surprisingly octopine also stimulated significant pAt15955
502 conjugation in the Ti^+At∆270 deletion strain (Figure 4). The Ti^-At∆270 derivative (IB132)
503 did not detectably conjugate, and conjugation in the At^+Ti^- strain (IB133) was the same
504 as the uninduced At^+ Ti^+, but was not stimulated by octopine addition. These findings
505 suggest that the pAt15955 can drive its own low-level conjugation, dependent on
506 conjugal transfer genes in the deleted segment (*trb* and *traI*). Octopine addition
507 stimulates pAt15955 conjugation and this is dependent on the Ti plasmid, and can even
508 overcome the absence of the pAt15955∆270 segment.

509 One explanation for pTi15955-dependent, octopine-induced transfer of pAt15955∆270
510 is cointegrate formation between pAt15955 and pTi15955 prior to Ti-driven conjugal
511 transfer. To determine whether both plasmids were transferred during conjugation
512 assays, pAt15955 transconjugants were screened for the presence of pTi15955 using
513 octopine auxotrophy screening and Eckhardt gel electrophoresis (Figure 5 and Figure
514 S7). As expected, donors possess pTi15955 and either pAt15955 (IB125) or
515 pAt15955∆270 (IB131), while the recipient (ERM52) is plasmidless (Figure 5).

516 Transconjugants from either donor show a mix of plasmid profiles; some have both
517 plasmids whereas others have only the pAt15955 or pAt15955Δ270 plasmids (Figure 5).
518 The transconjugants without the Ti plasmid are unlikely to have arisen due to co-
519 integrate formation, and for the pAt15955Δ270 plasmid the pTi15955-encoded conjugal
520 machinery can compensate for the missing *trb* and *traI* genes. However, because the
521 octopine-induced conjugation of pAt15955Δ270 appeared lower than pAt15955 (Figure
522 4), we tested whether the proportion of co-transfer of both plasmids was affected by the
523 pAt15955 segment, and found that it does not impact the co-transfer frequency (Figure
524 S7).

525 **pAt15955Δ270 segment deletion has environment-dependent fitness**
526 **consequences**

527 To determine whether the pAt15955 segment imposes fitness consequences that may
528 explain a propensity to lose the segment, competition experiments between isogenic
529 strains that either carry or have lost the pAt15955 segment were performed under
530 replete carbon, limiting carbon, and virulence-inducing conditions over nine serial
531 passages (Figure 6). In replete carbon conditions, there was not a measurable fitness
532 cost associated with the pAt15955Δ270 segment over the duration of the experiment. In
533 limiting carbon conditions, there was a modest, measurable fitness effect of the
534 segment that is similar to carriage costs determined for At plasmid deletions of a similar
535 size in *A. tumefaciens* C58 (Morton et al. 2013). In the high-stress, virulence-inducing
536 conditions, there was a significant fitness disadvantage to possessing the pAt15955
537 segment (Figure 6), suggesting that the presence of this region either increases general
538 susceptibility to the stressful conditions of virulence-induction or potentiates the *vir*

539 response under these conditions, both of which could result in a decrease of growth-
540 based fitness as measured in this assay.

541

542 **DISCUSSION**

543 Members of the family *Rhizobiaceae* exhibit signs of replicon co-evolution (Lassalle et
544 al. 2017, Slater et al. 2009, Wang et al. 2018) and cross-replicon interactions (Barnett et
545 al. 2004, Bobik et al. 2006, diCenzo et al. 2018, Galardini et al. 2015, Heidelberg et al.
546 2000, Pini et al. 2015, Ramachandran et al. 2017, Ronson et al. 1987), despite
547 remarkable strain-to-strain variation and the prevalence of large-scale rearrangements
548 in secondary replicons (Galardini et al. 2015, Lopez-Guerrero et al. 2012, Mazur et al.
549 2011, Morton et al. 2013, Orozco-Mosqueda Mdel et al. 2009). *A. tumefaciens* is a
550 member of this family and often carries a large proportion of its genomic DNA, including
551 important niche-associated functions, on two large extrachromosomal megaplasmids,
552 pAt and pTi (Goodner et al. 2001, Wood et al. 2001). Given the prevalence of both Ti
553 and At plasmids within *A. tumefaciens* isolates and bioinformatic evidence suggesting
554 co-evolution of these replicons (Lassalle et al. 2017), cross-replicon interactions are
555 likely to exist and in part function to co-stabilize the replicons. To this effect, we have
556 previously shown evidence of co-stability of both replicons in *A. tumefaciens* C58
557 (Morton et al. 2014), suggesting favorable interactions between both plasmids in some
558 strains.

559 Here, we show that curing of the Ti plasmid in the octopine-type strain *A. tumefaciens*
560 15955 drives a large deletion in the co-resident At plasmid, suggesting a discrete

561 genetic link between both plasmids that may underlie co-replicon stability. Our
562 observations suggested that the At plasmid was somehow limiting Ti curing. We
563 hypothesized that the Ti plasmid was being stabilized, perhaps through a toxin-
564 antitoxin-like interaction between both replicons, where a toxin (or other costly function)
565 on the At plasmid segment would be unchecked upon curing of the Ti plasmid.
566 Bioinformatic searches were able to identify multiple putative TA systems on the At
567 plasmid (Table S4), but none resided within the deletion segment and were actually
568 enriched outside of the segment, a distribution that might possibly contribute to the
569 dispensability of this region on pAt, but not explaining the propensity to lose the
570 pAt15955Δ270 segment under curing conditions. However, we found that deletion of
571 ~108 kb on the right half of this segment marginally increased pTi curing frequencies,
572 suggesting that the genetic content in this region does impact overall Ti plasmid
573 stability. The somewhat modest affect we observed provides evidence for cross-replicon
574 stability between both plasmids, and this may be exacerbated in certain environmental
575 conditions, but it seems unlikely that this observed stabilization explains the tight
576 correlation between pTi curing and At plasmid segment loss that we report here.

577 The deletion event itself is mediated by a repetitive IS-element, IS66, that flanks the At
578 segment and is required for its loss under curing conditions. IS66 was first identified on
579 the Ti plasmid of a different octopine-type strain of *A. tumefaciens* (Machida et al. 1984)
580 and is part of a larger family of IS-elements found within a variety of bacteria
581 (Gourbeyre et al. 2010, Han et al. 2001). IS-elements are common vehicles for genome
582 rearrangements and responsible for genome reduction in many bacterial taxa, including
583 species of *Bordatella* (Parkhill et al. 2003, Siguier et al. 2006). Ti plasmid curing could

584 conceivably elicit loss of the At plasmid segment through transposition of both flanking
585 IS66 elements in a mechanism similar to a composite transposon (Bellanger et al.
586 2014). However the observed retention of a single element at the site after deletion with
587 distint flanking duplications, and the tandem orientation of IS66 in full length pAt
588 suggests homologous recombination as the mechanism for At∆270 segment loss, and
589 hence should require RecA (Bell et al. 2016). Deletion of *recA* would clearly confirm
590 whether homologous recombination is required for loss of the At plasmid segment.
591 Whereas *recA* has been deleted previously in *A. tumefaciens* C58 (Farrand et al. 1989),
592 our repeated attempts at generating a similar deletion in *A. tumefaciens* 15955 were
593 unsuccessful (suggesting that the mutation is deleterious in 15955).

594 The IS66-mediated deletion observed here is different from another set of At plasmid
595 large deletions we have reported for *A. tumefaciens* C58, which appear to be mediated
596 by small repeat sequences (Morton et al. 2013). The low degree of At plasmid synteny
597 and the propensity of these plasmids to undergo large-scale rearrangements (Morton et
598 al. 2013) suggests that the fitness benefit of gene content on the At plasmid may be
599 highly environment-dependent. This is also true for the Ti plasmid, which imposes a
600 heavy fitness burden upon exposure to virulence-inducing conditions (Platt et al. 2012),
601 as well as other organisms, including species of *Methylobacterium*, where experimental
602 evolution resulted in an environment-dependent reduction of the accessory genome by
603 ~10% (Lee et al. 2012).

604 Genomic stability can be maintained in variety of ways, including the reduction of costs
605 associated with accessory genes (diCenzo et al. 2017). For example, the stability of Ti
606 plasmids is in part due to low carriage costs, low copy number, and extremely tight

607 regulation of costly genes, including virulence functions and conjugal transfer (Morton et
608 al. 2014, Pappas 2008, Pappas et al. 2003, Platt et al. 2012, Platt et al. 2012). The
609 current results have important consequences for our previous estimates of the low
610 carriage costs of the pTi15955 because these experiments unknowingly involved strains
611 that had incurred the pAt1599Δ270 kb deletion (Platt et al. 2012). In our previous work,
612 we concluded that under conditions which do not induce the Ti plasmid virulence genes
613 and are not substantially expressed, there was a low but measurable carriage cost
614 associated with pTi15955, while under virulence inducing conditions there was a large
615 cost associated with pTi15955. The findings reported here show that the measurement
616 of low, but significant basal carriage cost under non-inducing conditions reported in that
617 paper is likely a combination of costs associated with the Ti plasmid and costs
618 associated with the deleted At plasmid segment. The pAt15955Δ270 deletion alone
619 results in a significant fitness gain under similar experimental conditions (Figure 6) and
620 thus the carriage cost of the Ti plasmid reported in the previous paper is likely to be less
621 than estimated (Platt, Bever et al. 2012) and more similar to the low Ti plasmid carriage
622 costs we determined for pTiC58 from the nopaline-type *A. tumefaciens* strain C58
623 (Morton et al. 2014).

624 The At plasmid deletion observed here had significant effects on overall fitness in an
625 environment-dependent manner. While the segment conferred carriage costs similar to
626 At plasmid deletions we have characterized previously (Morton et al. 2013), the burden
627 of harboring the segment was significantly increased under virulence-inducing
628 conditions. Virulence genes are induced by a combination of low phosphate and acidic
629 pH, in addition to the presense of plant phenolics (Platt et al. 2012), so these conditions

630 are also highly stressful and may exacerbate the fitness cost of harboring this large
631 segment of the megaplasmid. However, the increased cost of this segment of pAt under
632 virulence induction also may suggest a role for the At plasmid in the response of *A.*
633 *tumefaciens* to the disease environment. This is consistent with our observations in *A.*
634 *tumefaciens* C58, where the At plasmid was found to modulate virulence gene
635 expression (Morton et al. 2013).

636 We identified additional interactions between these plasmids via their conjugal transfer
637 functions. We observed that pAt15955 conjugation exhibits a basal level of conjugation
638 that is further stimulated by the presence of octopine, the so-called conjugal opine for
639 many octopine-type Ti plasmids (Klapwijk et al. 1978). The basal conjugation of
640 pAt15955 in the absence of octopine is similar to that observed for the At plasmid of the
641 nopaline-type *A. tumefaciens* strain C58, in which pAtC58 conjugates constitutively
642 under laboratory conditions via its own conjugal transfer functions (Chen et al. 2002).
643 The predicted pTiC58 conjugal pilus is encoded by the *avhB* genes (*Agrobacterium*
644 virulence homologue *virB*), named as such due to their high homology to the pTiC58
645 plasmid-encoded VirB type IV secretion system which delivers T-DNA from *A.*
646 *tumefaciens* to plants during infection. The *avhB* genes are more distantly similar to the
647 pTiC58 conjugal pilus (*trb)* genes. In contrast, the pAt15955 *trb* genes within the At∆270
648 segment we describe here are more closely similar to the pTi15955 conjugal transfer
649 (*tra/trb*) genes then they are to *virB* genes on pTi15955. The basal conjugation of
650 pAt15955 is not affected by the presence of the pTi15955 plasmid, whereas the
651 presence of pTiC58 decreases pAtC58 conjugation by 10-fold (Chen et al. 2002).
652 However, activation of the pTiC58 *tra* genes was reported to stimulate pAtC58 conjugal

653 transfer (Lang et al. 2013). This was hypothesized to proceed through activation of the
654 *rctB* regulator of pAtC58 conjugal transfer functions. Interestingly, our genome
655 sequence reveals that pAt15955 has no *rctB*-type regulator and instead carries its own
656 paralogues of the Ti plasmid quorum sensing control genes, *traR* and *traM* on the
657 plasmid backbone, and the AHL synthese *traI* along with the *trb* genes, in the At∆270
658 segment. The TraR-TraI-TraM quorum sensing regulators on the Ti plasmid provide
659 strict octopine and population density-dependent control of pTi conjugation for octopine-
660 type Ti plasmids (Fuqua et al. 1995, Fuqua et al. 1996, Fuqua et al. 1994) and there is
661 some evidence that in a close relative of 15955, the strain *A. tumefaciens* A6, these
662 quorum sensing regulators may also regulate pAt conjugal transfer genes (Wang et al.
663 2014). The strong stimulation of pAt15955 by octopine, but only in the presence of the
664 Ti plasmid, suggests that octopine may trigger these regulators to increase *tra* gene
665 expression. Co-transfer of the At and Ti plasmid has been observed previously in the
666 plant tumor environment (Lang et al. 2013), but we show here that it is directly related to
667 octopine-induction of the Ti plasmid conjugation system and that both plasmid systems
668 interact. Intriguingly, independent, octopine-inducible transfer of the pAt15955 plasmid
669 that is missing the At∆270 segment which includes the *trb* and *traI* genes, only occurs in
670 the presence of pTi15955, suggesting that pAt15955 may also be able to utilize the Ti
671 *trb* functions for its own conjugation.

672 The genetic association between the At and Ti plasmids characterized here suggests
673 extensive cross-replicon interactions between these replicons that may underlie their
674 overall stability in changing environments. As a large proportion of bacteria possess
675 multiple large replicons, especially in *A. tumefaciens* and other members of

676 *Rhizobiaceae*, similar interactions are likely to occur in those systems and may exert a
677 profound influence on genomic stability. However, given the complex life histories
678 associated with many of these bacteria, it will be challenging to identify the relevant
679 environmental conditions which influence stability as well as the fitness costs associated
680 with large-scale rearrangements.

681

682 **ACKNOWLEDGEMENTS**

683 This work was supported by National Institutes of Health Grant [R01 GM092660 to C.F.
684 and J.D.B] and the Indiana Faculty Research Support Program (FRSP). We thank
685 James D. Bever (JDB) for serving as PI on the R01 grant. We also thank Grace Perkins
686 for technical assistance in the plasmid curing studies, Dean Rowe-Magnus for reagents
687 and advice for engineering large deletions using the Cre-*lox* system, and the Center for
688 Genomics and Bioinformatics at Indiana University for their work preparing the Illumina
689 libraries and operating the sequencing instrumentation.

690

REFERENCES

Agnoli, K et al. (2012). Exposing the third chromosome of *Burkholderia cepacia* complex strains as a virulence plasmid. Mol Microbiol 83(2): 362-378.

Bailey, J,Manoil, C (2002). Genome-wide internal tagging of bacterial exported proteins. Nat Biotechnol 20(8): 839-842.

Barnett, MJ, Toman, CJ, Fisher, RF,Long, SR (2004). A dual-genome Symbiosis Chip for coordinate study of signal exchange and development in a prokaryote–host interaction. Proc Natl Acad Sci, USA 101(47): 6.

Bell, JC,Kowalczykowski, SC (2016). RecA: Regulation and mechanism of a molecular search engine. Trends Biochem Sci 41(6): 491-507.

Bellanger, X, Payot, S, Leblond-Bourget, N,Guedon, G (2014). Conjugative and mobilizable genomic islands in bacteria: evolution and diversity. FEMS Microbiol Rev 38(4): 720-760.

Bobik, C, Meilhoc, E,Batut, J (2006). FixJ: a major regulator of the oxygen limitation response and late symbiotic functions of *Sinorhizobium meliloti*. J Bacteriol 188(13): 4890-4902.

Bolger, AM, Lohse, M,Usadel, B (2014). Trimmomatic: a flexible trimmer for Illumina sequence data. Bioinformatics 30(15): 2114-2120.

Carver, TJ et al. (2005). ACT: the Artemis Comparison Tool. Bioinformatics 21(16): 3422-3423.

Chain, PSG et al. (2006). *Burkholderia xenovorans* LB400 harbors amulti-replicon, 9.73-Mbp genome shaped for versatility. Proc Natl Acad Sci, USA 103(42): 8.

Chen, L, Chen, Y, Wood, DW,Nester, EW (2002). A new Type IV secretion system promotes conjugal transfer in *Agrobacterium tumefaciens*. Journal of Bacteriology 184(17): 4838-4845.

Deatherage, DE,Barrick, JE (2014). Identification of mutations in laboratory-evolved microbes from next-generation sequencing data using breseq. Methods Mol Biol 1151: 165-188.

diCenzo, GC,Finan, TM (2017). The divided bacterial genome: Structure, function, and evolution. Microbiol Mol Biol Rev 81(3).

diCenzo, GC et al. (2014). Examination of prokaryotic multipartite genome evolution through experimental genome reduction. PLoS Genet 10(10): e1004742.

diCenzo, GC, Wellappili, D, Golding, GB,Finan, TM (2018). Inter-replicon gene flow contributes to transcriptional integration in the *Sinorhizobium meliloti* multipartite genome. G3 (Bethesda) 8(5): 1711-1720.

Dougherty, K et al. (2014). Multiple phenotypic changes associated with large-scale horizontal gene transfer. PLoS One 9(7): e102170.

Eckhardt, T (1978). A rapid method for the identification of plasmid desoxyribonucleic acid in bacteria. Plasmid 1: 584-588.

Escobar, MA,Dandekar, AM (2003). *Agrobacterium tumefaciens* as an agent of disease. Trends Plant Sci. 8(8): 380-386.

Farrand, SK, O'Morchoe, SP,McCutchan, J (1989). Construction of an *Agrobacterium tumefaciens* C58 *recA* mutant. J Bacteriol 171(10): 8.

Finan, TM, Kunkel, B, De Vos, GF,Signer, ER (1986). Second symbiotic megaplasmid in *Rhizobium meliloti* carrying exopolysaccharide and thiamine synthesis genes. J Bacteriol 167(1): 7.

Funnell, BE,Phillips, GJ (2004). Plasmid Biology. Washington, D.C., ASM Press.

Fuqua, C, Burbea, M,Winans, SC (1995). Activity of the *Agrobacterium* Ti plasmid conjugal transfer regulator TraR is inhibited by the product of the *traM* gene. J Bacteriol 177(5): 7.

Fuqua, C,Winans, SC (1996). Conserved *cis*-acting promoter elements are required for density-dependent transcription of *Agrobacterium tumefaciens* conjugal transfer genes. J Bacteriol 178(2): 6.

Fuqua, WC,Weiner, RM (1993). The *melA* gene is essential for melanin biosynthesis in the marine bacterium *Shewanella colwelliana*. J Gen Microbiol. 139(5): 10.

Fuqua, WC,Winans, SC (1994). A LuxR-LuxI type regulatory system activates *Agrobacterium* Ti plasmid conjugal transfer in the presence of a plant tumor metabolite. J Bacteriol 176(10): 11.

Galardini, M et al. (2015). Evolution of intra-specific regulatory networks in a multipartite bacterial genome. PLoS Comput Biol 11(9): e1004478.

Galardini, M et al. (2013). Replicon-dependent bacterial genome evolution: the case of *Sinorhizobium meliloti*. Genome Biol Evol 5(3): 542-558.

González, M et al. (2005). The partitioned *Rhizobium etli* genome: Genetic and metabolic redundancy in seven interacting replicons. Proc Natl Acad Sci, USA 103(10): 6.

Goodner, B et al. (2001). Genome sequence of the plant pathogen and biotechnology agent *Agrobacterium tumefaciens* C58. Science 294(5550): 2323-2328.

Gordon, JE,Christie, PJ (2014). The *Agrobacterium* Ti plasmids. Microbiol Spectr 2(6).

Gourbeyre, E, Siguier, P,Chandler, M (2010). Route 66: Investigations into the organisation and distribution of the IS66 family of prokaryotic insertion sequences. Res Microbiol 161(2): 136-143.

Han, CG et al. (2001). Structural and functional characterization of IS679 and IS66-family elements. J Bacteriol 183(14): 4296-4304.

Heckel, BC et al. (2014). *Agrobacterium tumefaciens exoR* controls acid response genes and impacts exopolysaccharide synthesis, horizontal gene transfer, and virulence gene expression. J Bacteriol 196(18): 3221-3233.

Heidelberg, JF et al. (2000). DNA sequence of both chromosomes of the cholera pathogen *Vibrio cholera*e. Nature 406: 8.

Henkel, CV, den Dulk-Ras, A, Zhang, X,Hooykaas, PJ (2014). Genome sequence of the Octopine-type *Agrobacterium tumefaciens* strain Ach5. Genome Announc 2(2).

Huang, Y-Y et al. (2015). Complete Genome Sequence of *Agrobacterium tumefaciens* Ach5. Genome Announc 3(3): 2.

Hwang, I et al. (1994). TraI, a LuxI homologue, is responsible for production of conjugation factor, the Ti plasmid *N*-acylhomoserine lactone autoinducer. Proc Natl Acad Sci, USA 91: 5.

Klapwijk, PM, Scheulderman, T,Schilperoort, RA (1978). Coordinated regulation of octopine degradation and conjugative transfer of Ti plasmids in *Agrobacterium*

tumefaciens: Evidence for a common regulatory gene and separate operons. J Bacteriol 136(2): 11.

Kurtz, S et al. (2004). Versatile and open software for comparing large genomes. Genome Biol. 5(2): 9.

Lang, J et al. (2013). Concerted transfer of the virulence Ti plasmid and companion At plasmid in the *Agrobacterium tumefaciens*-induced plant tumour. Mol Microbiol.

Langmead, B,Salzberg, SL (2012). Fast gapped-read alignment with Bowtie 2. Nat Methods 9(4): 357-359.

Lassalle, F et al. (2017). Ancestral genome estimation reveals the history of ecological diversification in *Agrobacterium*. Genome Biol Evol 9(12): 3413-3431.

Lee, MC,Marx, CJ (2012). Repeated, selection-driven genome reduction of accessory genes in experimental populations. PLoS Genet 8(5): e1002651.

Lenski, R (1988). Experimental studies of pleiotropy and epistasis in *Escherichia coli*. I. Variation in competitive fitness among mutants resistant to virus T4. Evolution 42(3): 8.

Li, P-L, Everhart, DM,Farrand, SK (1998). Genetic and sequence analysis of the pTiC58 trb locus, encoding a mating-pair formation system related to members of the Type IV secretion family. J Bacteriol 180(23): 9.

Li, P-L, Hwang, I, Miyagi, H,Farrand, SK (1999). Essential components of the Ti plasmid *trb* system, a Type IV macromolecular transporter. J Bacteriol 181(16): 9.

Lopez-Guerrero, MG et al. (2012). Rhizobial extrachromosomal replicon variability, stability and expression in natural niches. Plasmid 68(3): 149-158.

Machida, Y et al. (1984). Nucleotide sequence of the insertion sequence found in the T-DNA region of mutant Ti plasmid pTiA66 and distribution of its homologues in octopine Ti plasmid. Proc Natl Acad Sci, U S A 81: 5.

Mauchline, TH et al. (2014). Mapping the *Sinorhizobium meliloti* 1021 solutebinding protein-dependent transportome. Proc Natl Acad Sci, USA 103(47): 6.

Mazur, A et al. (2011). Intragenomic diversity of *Rhizobium leguniosarum* bv. trifolii clover nodule isolates. BMC Microbiol 11: 123.

Morton, ER,Fuqua, C (2012). Genetic manipulation of *Agrobacterium*. Curr Protoc Microbiol: Unit 3D 2.

Morton, ER,Fuqua, C (2012). Laboratory maintenance of *Agrobacterium*. Curr Protoc Microbiol: Unit3D 1.

Morton, ER, Merritt, PM, Bever, JD,Fuqua, C (2013). Large deletions in the pAtC58 megaplasmid of *Agrobacterium tumefaciens* can confer reduced carriage cost and increased expression of virulence genes. Genome Biol Evol 5(7): 1353-1364.

Morton, ER, Platt, TG, Fuqua, C,Bever, JD (2014). Non-additive costs and interactions alter the competitive dynamics of co-occurring ecologically distinct plasmids. Proc Biol Sci 281(1779): 20132173.

Mougel, C, Thioulouse, J, Perrière, G,Nesme, X (2002). A mathematical method for determining genome divergence and species delineation using AFLP. Int. J. Syst. Evol. Microbiol. 52: 14.

Orozco-Mosqueda Mdel, C et al. (2009). Homologous recombination and dynamics of rhizobial genomes. Res Microbiol 160(10): 733-741.

Pappas, KM (2008). Cell-cell signaling and the *Agrobacterium tumefaciens* Ti plasmid copy number fluctuations. Plasmid 60(2): 89-107.

Pappas, KM,Winans, SC (2003). A LuxR-type regulator from *Agrobacterium tumefaciens* elevates Ti plasmid copy number by activating transcription of plasmid replication genes. Mol Microbiol 48(4): 15.

Parkhill, J et al. (2003). Comparative analysis of the genome sequences of *Bordetella pertussis*, *Bordetella parapertussis* and *Bordetella bronchiseptica*. Nat Genet 35(1): 32-40.

Petes, TD,Hill, CW (1988). Recombination between repeated genes in microorganisms. Annu Rev Genet 22: 22.

Pini, F et al. (2015). Cell cycle control by the master regulator CtrA in *Sinorhizobium meliloti*. PLoS Genet 11(5): e1005232.

Piper, KR, Beck von Bodman, S,Farrand, SK (1993). Conjugation factor of *Agrobacterium tumefaciens* regulates Ti plasmid transfer by autoinduction. Nature 362(1): 3.

Platt, TG, Bever, JD,Fuqua, C (2012). A cooperative virulence plasmid imposes a high fitness cost under conditions that induce pathogenesis. Proc Biol Sci 279(1734): 1691-1699.

Platt, TG, Fuqua, C,Bever, JD (2012). Resource and competitive dynamics shape the benefits of public goods cooperation in a plant pathogen. Evolution 66(6): 1953-1965.

Platt, TG et al. (2014). Ecological dynamics and complex interactions of *Agrobacterium* megaplasmids. Front Plant Sci 5: 635.

Ramachandran, R, Jha, J, Paulsson, J,Chattoraj, D (2017). Random versus cell cycle-regulated replication initiation in bacteria: insights from studying *Vibrio cholerae c*hromosome 2. Microbiol Mol Biol Rev 81(1).

Romanchuk, A et al. (2014). Bigger is not always better: Transmission and fitness burden of ∼1 MB *Pseudomonas syringae* megaplasmid pMPPla107. Plasmid 73: 10.

Ronson, CW, Nixon, BT, Albricht, LM,Ausubel, FM (1987). *Rhizobium meliloti ntrA* (*rpoN*) gene is required for diverse metabolic functions. J Bacteriol 169(6): 8.

Siguier, P, Filee, J,Chandler, M (2006). Insertion sequences in prokaryotic genomes. Curr Opin Microbiol 9(5): 526-531.

Slater, SC et al. (2009). Genome sequences of three agrobacterium biovars help elucidate the evolution of multichromosome genomes in bacteria. J Bacteriol 191(8): 2501-2511.

Suzuki, K, Iwata, K,Yoshida, K (2001). Genome analysis of *Agrobacterium tumefaciens*: construction of physical maps for linear and circular chromosomal dnas, determination of copy number ratio and mapping of chromosomal virulence genes. DNA *Res* 8: 12.

Uraji, M, Suzuki, K,Yoshida, K (2002). A novel plasmid curing method using incompatibility of plant pathogenic Ti plasmids in *Agrobacterium tumefaciens*. Genes Genet. Syst. 77: 1-9.

Uraji, M, Suzuki, K., and Yoshida, K. (2002). A novel plasmid curing method using incompatibility of plant pathogenic Ti plasmids in *Agrobacterium tumefaciens*. Genes Genet. Syst. 77: 1-9.

Van Larebeke, N et al. (1974). Large plasmid in *Agrobacterium tumefaciens* essential for crown gall-inducing ability. Nature 252: 10.

Wang, C, Yan, C, Fuqua, C,Zhang, LH (2014). Identification and characterization of a second quorum-sensing system in *Agrobacterium tumefaciens* A6. J Bacteriol 196(7): 1403-1411.

Wang, X et al. (2018). Comparative analysis of rhizobial chromosomes and plasmids to estimate their evolutionary relationships. Plasmid 96-97: 13-24.

Watson, B et al. (1975). Plasmid required for virulence of *Agrobacterium tumefaciens*. J Bacteriol 123: 10.

Wood, DW et al. (2001). The Genome of the Natural Genetic Engineer *Agrobacterium tumefaciens* C58. Science 294: 8.

Xie, Y et al. (2018). TADB 2.0: an updated database of bacterial type II toxin-antitoxin loci. Nucleic Acids Res 46(D1): D749-D753.

Yamamoto, S et al. (2018). Effective removal of a range of Ti/Ri plasmids using a pBBR1-type vector having a repABC operon and a lux reporter system. Appl Microbiol Biotechnol 102(4): 1823-1836.

Table 1: pAt15955 segment deletion and pTi15955 curing frequencies under incompatibility-based pTi15955 curing conditions.

Strain	Genotype		Ti curing conditions	
	pAT	pTi	At deletion freq.[a]	Ti curing freq.[b]
WT (IB118/IB126)[c]	+	+	0.71 ± 0.10	0.28 ± 0.08
IB118 ΔIS66	+	+	< 3.0 x 10^{-8}	Not determined
IB129	Δ270	+ (RI)[d]	NA	0.45 ± 0.17
IB130	+	+ (RI)[d]	Not determined	0.13 ± 0.08
IB118 ΔL	Δ130 L	+	Not determined	0.27 ± 0.04
IB118 ΔR	Δ130 R	+	Not determined	0.42 ± 0.17
IB118 ΔL+R	Δ270	+	NA	0.39 ± 0.07

[a]At deletion frequency determined as the ratio of *A. tumefaciens* curing plasmid transconjugants that have incurred the At plasmid deletion to total transconjugants.

[b]Ti curing frequency determined as the ratio of *A. tumefaciens* curing plasmid transconjugants that have lost the Ti plasmid to total transconjugants. ~100% of isolates

cured for pTi15955 have also incurred the pAt15955Δ270 deletion and only rare isolates have been recovered that retain the segment upon pTi15955 curing (text and Table S1).

[c]WT represents combined data from IB118 and IB126 for At deletion and Ti curing frequencies.

[d]RI – indicates that pTi15955 was re-introduced by conjugation

FIGURE LEGENDS

Figure 1: Multiple changes in plasmid profile of *A. tumefaciens* 15955 upon curing of pTi15955. Eckhardt gel electrophoresis analysis of WT *A. tumefaciens* 15955 and two derivatives of *A. tumefaciens* 15955, cured of the Ti plasmid (pTi15955) using either chemical (SA122) or plasmid incompatibility methods (IB124). Positions of pAt15955 and pTi15955 in WT *A. tumefaciens* 15955 are shown. Arrow indicates single band present in pTi15955-cured derivatives.

Figure 2: Whole genome sequencing confirms co-incident pAt15955 deletion upon pTi15955 curing. Mummerplot visualization of MUMmer 3 alignment of genome assembly scaffolds from WT 15955 (X axis) and a pTi15955-cured derivative (IB124, Y axis) confirm loss of a large, ~270 Kbp segment in pAt15955 upon pTi15955 curing. Matching sequence between assemblies is indicated with diagonal red line segments. Sequence corresponding to each replicon is indicated. Inset (dashed) highlights large (270 Kbp) deletion of pAt15955 and absence of pTi15955 in IB124.

Figure 3: Loss of one IS66 element upon deletion of ~270 Kbp pAt15955 segment. Southern blot analysis of gDNA from WT *A. tumefaciens* 15955 (**A**) and two derivatives that have either incurred loss of the pAt15955 segment (IBE13A, **B**) or pTi15955 (IBJUN138, **C**) using three restriction enzyme digests that do not cleave within IS66 (SphI, EcoRI, and BamHI). Ladder shown is NEB 1 kb DNA ladder. Numbers on Y-axis indicated ladder sizes in Kbp. **D)** Bioinformatic prediction of IS66-containing restriction

fragment sizes for digests in A, B, and C – color coding matches the dots adjacent to each band. In A and C, two hybridizing fragments correspond to IS66 elements flanking pAt15955 segment and one to IS66 on the linear chromosome. In B, one hybridizing fragment corresponds to the linear chromosome and one to the remaining fragment to IS66 on pAt15955Δ270 at deletion site.

Figure 4: Octopine-inducible pAt15955 conjugation is pTi15955-dependent and independent of pAt15955-encoded *trb* machinery. pAt15955 conjugation frequencies of marked (Km^R) derivatives of *A. tumefaciens* 15955 into a plasmidless recipient, ERM52, under standard growth (ATGN, dark gray) and octopine-containing (ATGNO, hatched, 3.25 mM) conditions. Strains shown are WT (IB125) or derivatives deleted for pAt15955 segment (IB131), pTi15955 (IB133), or both (IB132). Conjugation frequencies reported as transconjugants per output donor (Methods). A and B denote p-value <0.03.

Figure 5: Co-transfer of pTi15955 in pAt15955 transconjugants in the presence of octopine. Plasmid profiles for subset of pAt15955 transconjugants from conjugation assay in Figure 4 were determined by Eckhardt gel electrophoresis. Shown are profiles for two donors (IB125 and IB131), recipient (ERM52), and three transconjugants from conjugation assays with either donor (IB125 or IB131). Indicated below gel image are presence (+) or absence (-) of pTi15955 and the presence of WT pAt15955 (+) or pAt15955Δ270 (Δ270).

Figure 6: pAt15955 segment loss confers an environment-dependent fitness advantage. Relative fitness of WT *A. tumefaciens* 15955 and a strain isogenic for loss of the pAt15955 segment over one (P0-P1), five (P0-P5) and nine (P0-P9) serial passages in replete carbon (dark gray), limiting carbon (hatched), and virulence-inducing conditions (white). Bars represent 6 biological replicates, 3 each with inversely marked strains (Methods). Relative fitness calculated as the total number of doublings of each competitor over the indicated passing interval (Methods). Error bars shown are standard deviation. Asterisk indicates p-value < 0.05 in comparison to the expectation of 1.

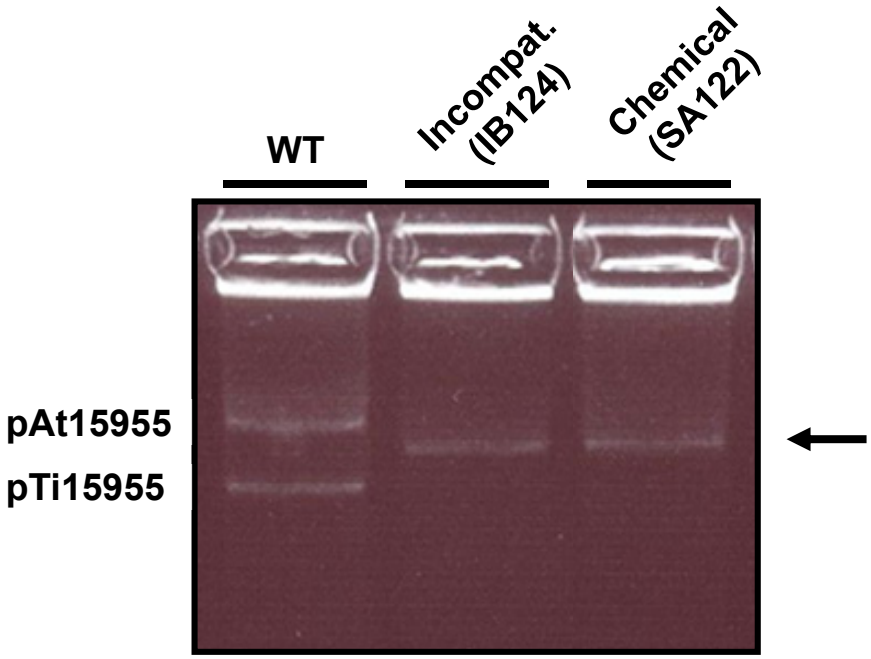

Figure 1: Multiple changes in plasmid profile of *A. tumefaciens* 15955 upon curing of pTi15955. Eckhardt gel electrophoresis analysis of WT *A. tumefaciens* 15955 and two derivatives of *A. tumefaciens* 15955, cured of the Ti plasmid (pTi15955) using either chemical (SA122) or plasmid incompatibility methods (IB124). Positions of pAt15955 and pTi15955 in WT *A. tumefaciens* 15955 are shown. Arrow indicates single band present in pTi15955-cured derivatives.

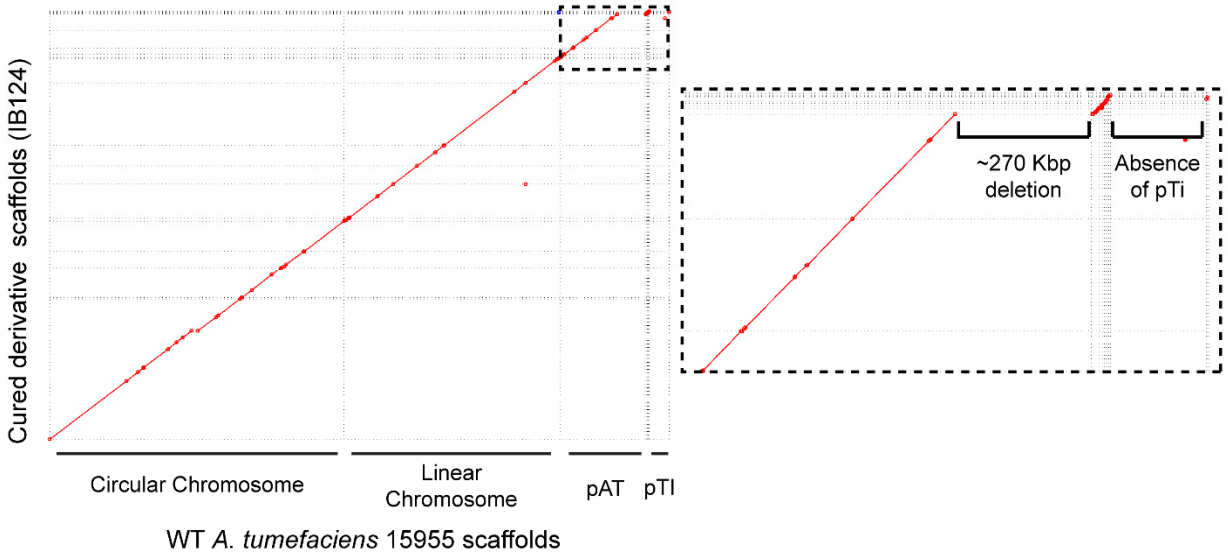

Figure 2: Whole genome sequencing confirms co-incident pAt15955 deletion upon pTi15955 curing. Mummerplot visualization of MUMmer 3 alignment of genome assembly scaffolds from WT 15955 (X axis) and a pTi15955-cured derivative (IB124, Y axis) confirm loss of a large, ~270 Kbp segment in pAt15955 upon pTi15955 curing. Matching sequence between assemblies is indicated with diagonal red line segments. Sequence corresponding to each replicon is indicated. Inset (dashed) highlights large (270 Kbp) deletion of pAt15955 and absence of pTi15955 in IB124.

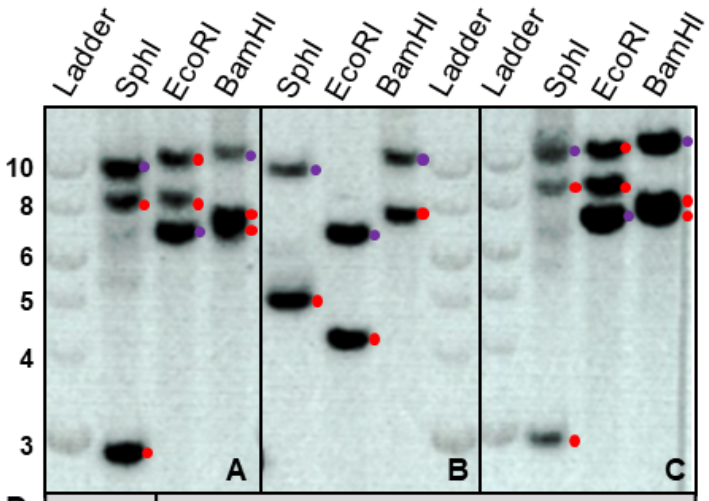

D

Panel	Predicted fragment sizes (Kbp)		
	SphI	EcoRI	BamHI
A	9.9, 8.1, 2.8	10.3, 8.2, 6.6	10.3, 6.8, 7.2
B	9.9, 4.9	6.6, 4.1	10.3, 7.3
C	9.9, 8.1, 2.8	10.3, 8.2, 6.6	10.3, 6.8, 7.2

Figure 3: Loss of one IS66 element upon deletion of ~270 Kbp pAt15955 segment. Southern blot analysis of gDNA from WT *A. tumefaciens* 15955 (**A**) and two derivatives that have either incurred loss of the pAt15955 segment (IBE13A, **B**) or pTi15955 (IBJUN138, **C**) using three restriction enzyme digests that do not cleave within IS66 (SphI, EcoRI, and BamHI). Ladder shown is NEB 1 kb DNA ladder. Numbers on Y-axis indicated ladder sizes in Kbp. **D)** Bioinformatic prediction of IS66-containing restriction fragment sizes for digests in A, B, and C – color coding matches the dots adjacent to each band. In A and C, two hybridizing fragments correspond to IS66 elements flanking pAt15955 segment and one to IS66 on the linear chromosome. In B, one hybridizing fragment corresponds to the linear chromosome and one to the remaining fragment to IS66 on pAt15955Δ270 at deletion site.

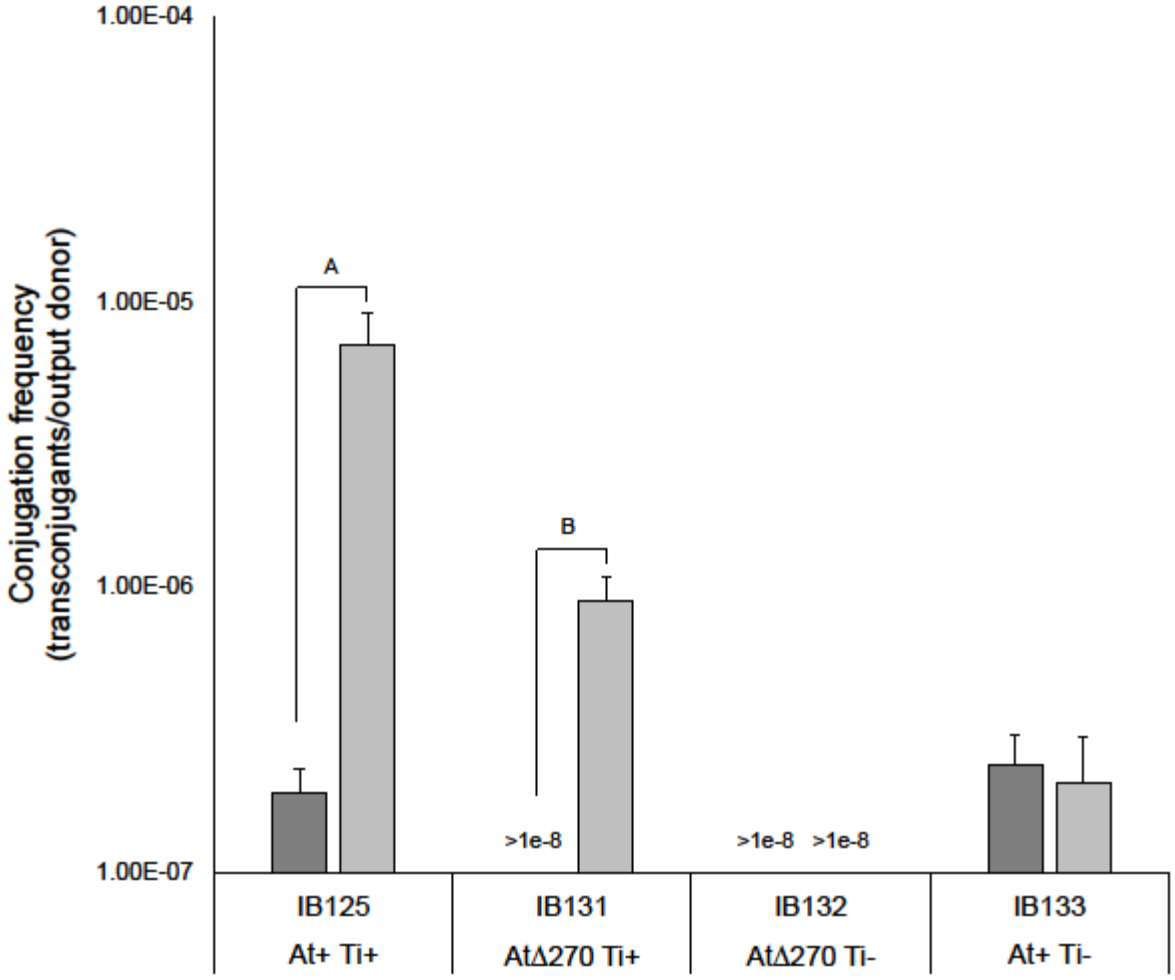

Figure 4: Octopine-inducible pAt15955 conjugation is pTi15955-dependent and independent of pAt15955-encoded *trb* machinery. pAt15955 conjugation frequencies of marked (Km^R) derivatives of *A. tumefaciens* 15955 into a plasmidless recipient, ERM52, under standard growth (ATGN, dark gray) and octopine-containing (ATGNO, hatched, 3.25 mM) conditions. Strains shown are WT (IB125) or derivatives deleted for pAt15955 segment (IB131), pTi15955 (IB133), or both (IB132). Conjugation frequencies reported as transconjugants per output donor (Methods). A and B denote p-value <0.03.

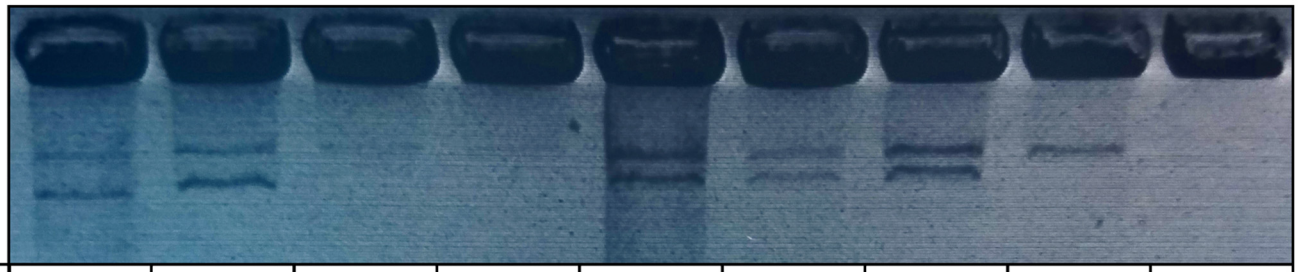

	Donor (IB125)	Transconjugants (IB125)			Donor (IB131)	Transconjugants (IB131)			Recip. (ERM52)
pAt	+	+	+	+	Δ270	Δ270	Δ270	Δ270	-
pTi	+	+	-	-	+	+	+	-	-

Figure 5: Co-transfer of pTi15955 in pAt15955 transconjugants in the presence of octopine. Plasmid profiles for subset of pAt15955 transconjugants from conjugation assay in Figure 4 were determined by Eckhardt gel electrophoresis. Shown are profiles for two donors (IB125 and IB131), recipient (ERM52), and three transconjugants from conjugation assays with either donor (IB125 or IB131). Indicated below gel image are presence (+) or absence (-) of pTi15955 and the presence of WT pAt15955 (+) or pAt15955Δ270 (Δ270).

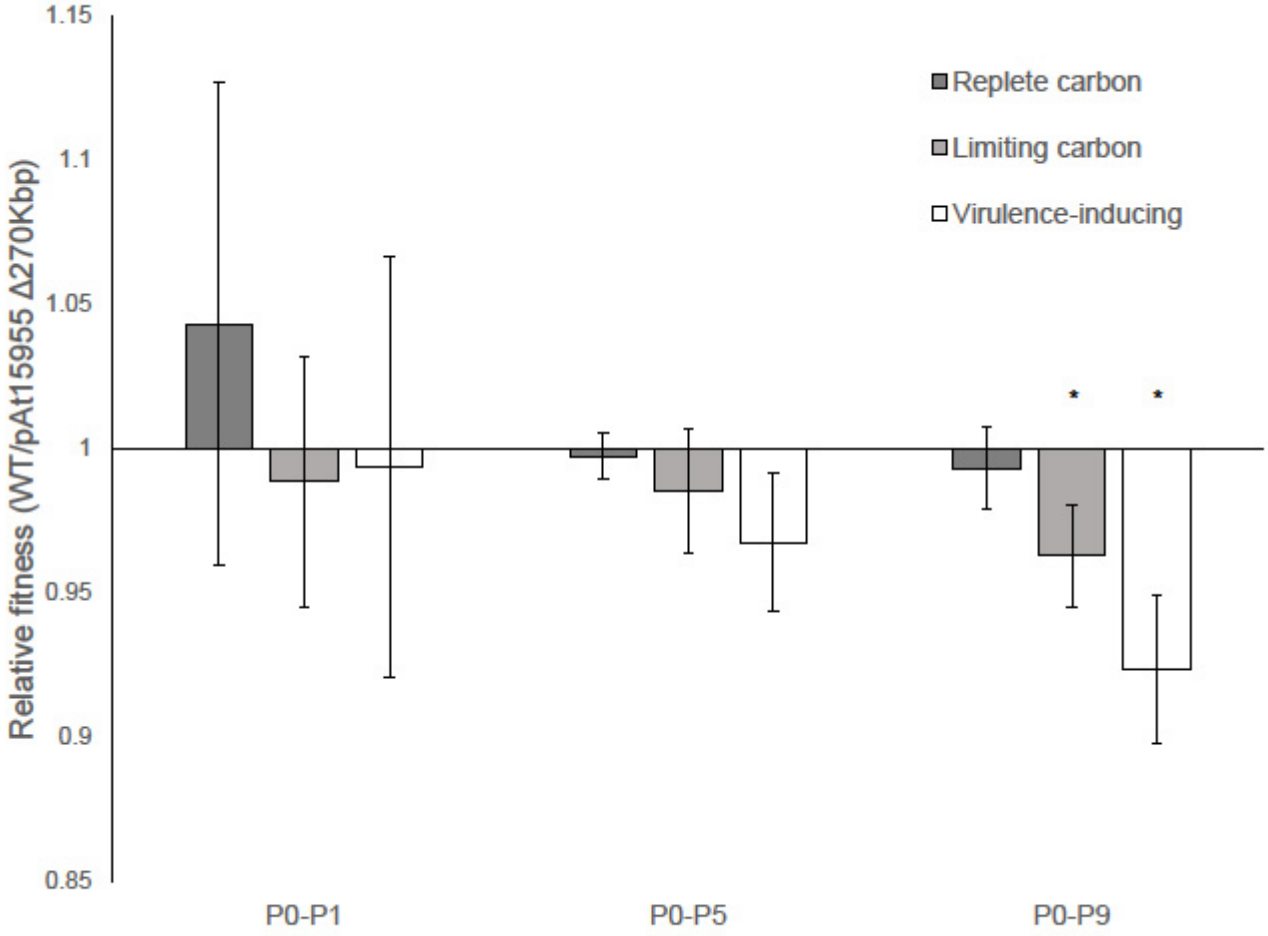

Figure 6: pAt15955 segment loss confers an environment-dependent fitness advantage. Relative fitness of WT *A. tumefaciens* 15955 and a strain isogenic for loss of the pAt15955 segment over one (P0-P1), five (P0-P5) and nine (P0-P9) serial passages in replete carbon (dark gray), limiting carbon (hatched), and virulence-inducing conditions (white). Bars represent 6 biological replicates, 3 each with inversely marked strains (Methods). Relative fitness calculated as the total number of doublings of each competitor over the indicated passing interval (Methods). Error bars shown are standard deviation. Asterisk indicates p-value < 0.05 in comparison to the expectation of 1.